UC Berkeley

UC Berkeley Previously Published Works

Title

Tests of redshift-space distortions models in configuration space for the analysis of the BOSS final data release

Permalink

https://escholarship.org/uc/item/2k62w6jj

Journal

Monthly Notices of the Royal Astronomical Society, 447(1)

ISSN

0035-8711

Authors

White, Martin
Reid, Beth
Chuang, Chia-Hsun
et al.

Publication Date

2015-02-11

DOI

10.1093/mnras/stu2460

Peer reviewed

eScholarship.org Powered by the California Digital Library
University of California

Mon. Not. R. Astron. Soc. **000**, 1–13 (0000) Printed 27 November 2014 (MN LATEX style file v2.2)

Tests of redshift-space distortions models in configuration space for the analysis of the BOSS final data release

Martin White[1,2], Beth Reid[2], Chia-Hsun Chuang[3], Jeremy L. Tinker[4], Cameron K. McBride[5], Francisco Prada[3,6,7], Lado Samushia[8,9]

[1] *Departments of Physics and Astronomy, University of California, Berkeley, CA 94720, USA*
[2] *Lawrence Berkeley National Laboratory, 1 Cyclotron Road, Berkeley, CA 94720, USA*
[3] *Instituto de Física Teórica, (UAM/CSIC), Universidad Autónoma de Madrid, Cantoblanco, E-28049 Madrid, Spain*
[4] *Center for Cosmology and Particle Physics, New York University, New York, NY 10003, USA*
[5] *Harvard-Smithsonian Center for Astrophysics, 60 Garden St., Cambridge, MA 02138, USA*
[6] *Campus of International Excellence UAM+CSIC, Cantoblanco, E-28049 Madrid, Spain*
[7] *Instituto de Astrofísica de Andalucía (CSIC), Glorieta de la Astronomía, E-18080 Granada, Spain*
[8] *Department of Physics, Kansas State University, 116 Cardwell Hall, Manhattan, KS 66506, USA*
[9] *National Abastumani Astrophysical Observatory, Ilia State University, 2A Kazbegi Ave., GE-1060 Tbilisi, Georgia*

arXiv:1408.5435v3 [astro-ph.CO] 26 Nov 2014

27 November 2014

ABSTRACT

Observations of redshift-space distortions in spectroscopic galaxy surveys offer an attractive method for observing the build-up of cosmological structure, which depends both on the expansion rate of the Universe and our theory of gravity. In preparation for analysis of redshift-space distortions from the Baryon Oscillation Spectroscopic Survey (BOSS) final data release we compare a number of analytic and phenomenological models, specified in configuration space, to mock catalogs derived in different ways from several N-body simulations. The galaxies in each mock catalog have properties similar to those of the higher redshift galaxies measured by BOSS but differ in the details of how small-scale velocities and halo occupancy are determined. We find that all of the analytic models fit the simulations over a limited range of scales while failing at small scales. We discuss which models are most robust and on which scales they return reliable estimates of the rate of growth of structure: we find that models based on some form of resummation can fit our N-body data for BOSS-like galaxies above $30\,h^{-1}$Mpc well enough to return unbiased parameter estimates.

Key words: gravitation; galaxies: haloes; galaxies: statistics; cosmological parameters; large-scale structure of Universe

1 INTRODUCTION

The evolution of our Universe appears to be well described by Einstein's theory of General Relativity. The large-scale structure within it is understood as the consequence of gravitational instability, which amplifies primordial fluctuations laid down at early times. Within this paradigm, the growth of large-scale structure is driven by the motion of matter and inhibited by the cosmological expansion. Once the content, spatial geometry and initial perturbations in the Universe are specified, Einstein's theory makes precise predictions for the expansion rate and, simultaneously, the rate of growth of large-scale structure. These predictions can be compared with observations made in galaxy redshift surveys to test the theory and to provide constraints on the parameters of our cosmological model. We can measure the velocity field from maps of galaxies in such surveys because the galaxy redshifts, from which distances are inferred, include components from both the Hubble flow and peculiar velocities from the comoving motions of galaxies (see Hamilton 1998 for a review). Thus even though the statistics of the galaxy distribution are isotropic, redshift surveys exhibit an anisotropic distribution. The anisotropy encodes information about the build-up of structure and provides a sharp test of the theory (see e.g. Berlind, Narayanan & Weinberg 2001; Zhang et al. 2007; Jain & Zhang 2008; Guzzo et al. 2008; Neseris & Perivolaropoulos 2008; Song & Koyama 2009; Song & Percival 2009; Percival & White 2008; McDonald & Seljak 2009; White, Song & Percival 2009; Song et al. 2010; Zhao et al. 2010; Song et al. 2011, for recent studies).

The measured anisotropy of the clustering of galaxies seen in redshift surveys combines virial motions within halos on small-scales (Jackson 1972) and supercluster-infall on large scales (Kaiser 1987). Over the past two decades the measurement of these effects has become increasingly precise (Cole, Fisher & Weinberg 1995; Peacock et al. 2001; Percival et al. 2004; da Angela et al. 2008; Okumura et al. 2008; Guzzo et al. 2008; Blake et al. 2011; Samushia, Percival, & Raccanelli 2012; Reid et al. 2012; Samushia et al. 2013; Blake et al. 2013; de la Torre et al. 2013; Samushia et al.

© 0000 RAS

2014; Sanchez et al. 2014; Bel et al. 2014; Tojeiro et al. 2014). Reliably extracting cosmological information from such precise measurements requires models which are accurate, to the level of the data uncertainties, on the scales over which they are fitted. In this paper we compare how well a number of different models recover the growth rate in mock catalogs made from N-body simulations, in order to delineate the range of validity of the models in preparation for using them to analyze data from the final release of data from the Baryon Oscillation Spectroscopic Survey (BOSS; Dawson et al. 2013), which is part of Sloan Digital Sky Survey III (SDSS-III; Eisenstein et al. 2011). To this end we have developed a number of mock galaxy catalogs with clustering properties similar to those of the higher redshift BOSS galaxies. While having similar clustering and number density, the mock catalogs differ in detail and have been generated to test various aspects of the redshift-space distortion (RSD) models.

Our focus in this paper is on a set of analytic and phenomenological models described in configuration space (and described further in Section 2, see also Okumura & Jing 2011; de la Torre & Guzzo 2012; Bianchi et al. 2012; Gil-Marin et al. 2012 and references below). Recent, complementary, tests of models in Fourier space have been presented in Jennings, Baugh & Pascoli (2011); Blake et al. (2011); Kwan, Lewis & Linder (2012); Okumura, Seljak & Descjacques (2012); Zheng et al. (2013); Okumura et al. (2014); Beutler et al. (2014) and N-body based models for fitting the data to smaller scales have been presented in Reid et al. (2014). The outline of the paper is as follows. In Section 2 we introduce the models we will be considering and the parameters upon which they depend. In Section 3 we describe the N-body simulations and mock catalogs which we shall use as a reference for the models to fit. Section 4 describes our methodology and we discuss the implications in Section 5.

2 MODELS

In this section we describe the models which we shall fit to the N-body data, with a focus on models which make predictions in configuration space (recent, complementary tests of models in Fourier space have been presented in the papers cited above). The first two models are "dispersion models", which Scoccimarro (2004) showed inherently assume an unphysical pairwise velocity distribution. The second two models express the redshift-space correlation function as an integral of the real-space correlation function times a pairwise velocity distribution function.

Throughout we adopt the standard "plane-parallel" or "distant-observer" approximation, in which the line-of-sight direction to each object is taken to be the fixed direction $\hat{z}$. This has been shown to be a good approximation at the level of current observational error bars (e.g., Figure 10 of Samushia, Percival, & Raccanelli 2012 or Figure 8 of Yoo & Seljak 2014).

2.1 The Eulerian dispersion model

The simplest model for redshift space distortions combines the supercluster infall enhancement of Kaiser (1987) with an independent small-scale suppression to account for the virial motions of satellites in halos (the finger-of-god effect). In Fourier space the assumption of an exponential pairwise velocity distribution with a scale-independent width, along with the linear theory relation for supercluster infall, leads to (Peacock 1992; Park et al. 1994; Peacock & Dodds 1994; Ballinger, Peacock & Heavens 1996; Hamilton 1998; Hatton & Cole 1999):

$$P(k,\mu) = P_r(k)\frac{(b+f\mu^2)^2}{1+k^2\mu^2\sigma_E^2} \quad (1)$$

where σ_E is a free parameter to be fit to the data, b is the large-scale (assumed scale-independent) bias and $f = d\ln\delta/d\ln a \approx \Omega_m^{0.55}(z)$ is the growth rate of perturbations. A motivation for the exponential form of the pairwise velocity distribution can be found in White (2001); Seljak (2001), expressions for the Legendre moments of Eq. (1) can be found in Cole, Fisher & Weinberg (1995). The exact form of the small-scale suppression, and the value of σ_E, are strongly dependent on the galaxy population being modeled (Jing & Börner 2004; Li et al. 2007). Sometimes a model with $(1+k^2\mu^2\sigma_E^2/2)^2$ in the denominator is used; this agrees with Eq. (1) for low k. An alternative formulation is to take the high-k damping term as a Gaussian, $\exp[-k^2\mu^2\sigma_E^2]$. Again the expressions match for low k.

In Eq. (1) we can use the linear theory power spectrum, or we can use a model for the non-linear power spectrum (but ignoring non-linear bias and the generic perturbation theory differences in the non-linear evolution of velocity and density). In the study of Blake et al. (2011), Eq. (1) with a non-linear power spectrum calculated as in Smith et al. (2003) performed very well against data when fitted in Fourier space. We shall consider both the linear and non-linear forms, referring to the former as the Eulerian Dispersion Model (EDM) and the latter as the Non-linear Dispersion Model (NDM) (following Peebles 1980; Fisher 1995). Tinker, Weinberg & Zheng (2006) and Tinker (2007), which are developments of the work in Hatton & Cole (1999), discuss a number of improvements to models like this based on fits to numerical simulation results. We shall not consider these improvements, since the original form is the most widely used.

The correlation function, which shall be the primary focus of this paper, is the Fourier transform of this power spectrum. If we expand the correlation function in Legendre polynomials, L_ℓ,

$$\xi(s,\widehat{s}\cdot\widehat{z}) = \sum_\ell \xi_\ell(s) L_\ell(\widehat{s}\cdot\widehat{z}) \quad (2)$$

where $\mathbf{s}$ is the redshift-space coordinate, then

$$\xi_\ell(s) = (2\ell+1)i^\ell \int \frac{d^3k}{(2\pi)^3} P(k,\mu) L_\ell(\mu) j_\ell(ks) \quad (3)$$

where j_ℓ is a spherical Bessel function of order ℓ. We shall restrict our attention to the lowest non-vanishing moments, $\ell = 0$ and 2.

This model has three free parameters, which we can take to be either $b\sigma_8$, $f\sigma_8$ and σ_E or b, f and σ_E depending on whether we wish to treat the linear theory power spectrum amplitude as known.

We note that the model of Chuang et al. (2013) is almost the same as the EDM, differing only in the modeling of the acoustic peak region. Since the acoustic feature has very little weight in our fits we expect our discussion of the EDM will apply approximately to this model as well.

2.2 Perturbation theory inspired model

We also consider a model inspired by, but not directly derived from, perturbation theory in combination with the reasoning described above. We call this model the perturbation-inspired model (PIM). It was used to interpret the BOSS data in Sanchez et al. (2013,

2014). This model assumes

$$P(k,\mu) = \left(\frac{b + f\mu^2}{1 + k^2 f^2 \sigma_P^2 \mu^2}\right)^2 \left[e^{-k^2\sigma_P^2} P_{\rm lin}(k) + A\, P_{22}(k)\right] \quad (4)$$

where b, f, σ_P and A are free parameters and P_{22} is the standard second-order, mode-coupling term in Eulerian perturbation theory (Peebles 1980; Juszkiewicz 1981; Vishniac 1983; Goroff et al. 1986; Makino et al. 1992; Jain & Bertschinger 1994). For further details on, and tests of, the model see Sanchez et al. (2013, 2014). In comparison with the other models note the factors of f in the prefactor, the squaring of the finger-of-god term, the double duty played by the parameter σ_P and the isotropic nature of the broadening of the acoustic peak (i.e. the exponential multiplying $P_{\rm lin}$). As it stands this model has one additional parameter (A) that can be varied in the fit beyond the large-scale bias, b and σ_P.

2.3 The Gaussian streaming model

The "Gaussian streaming model" (GSM) was developed in Reid & White (2011); Reid et al. (2012), where it was shown to fit the monopole and quadrupole of the correlation functions of mock galaxies with a large-scale bias $b \simeq 2$ to the per cent level on scales above $25\,h^{-1}$Mpc. This model has been used to interpret the clustering of galaxies measured in BOSS by Reid et al. (2012); Samushia et al. (2013, 2014). The GSM is inspired by the work of Peebles (1980); Fisher (1995). The pairwise velocity distribution is different for components along and perpendicular to the (real space) pair separation vector $\widehat{rr}$, with the mean pairwise velocity $v_{12}(r)\widehat{r}$ oriented along $\widehat{r}$. The mean and variance of the pairwise velocity distribution for the line-of-sight (LOS) velocity component therefore depends on $\mu_r = \widehat{r}\cdot\widehat{z}$. The GSM approximates the pairwise velocity distribution as Gaussian and enforces pair conservation by integrating over all possible real space LOS pair separations y that appear at redshift space separation $s_\parallel$. Specifically we assume that the redshift-space halo correlation function is

$$1 + \xi^s(s_\perp, s_\parallel) = \int \frac{dy}{\sqrt{2\pi}\sigma_{12}} [1 + \xi(r)] \exp\left\{-\frac{[s_\parallel - y - \mu_r v_{12}]^2}{2\sigma_{12}^2}\right\}, \quad (5)$$

where $\xi(r)$, v_{12} and σ_{12} are to be provided from an analytic theory. In its basic form (Reid & White 2011; Reid et al. 2012) integrated Lagrangian perturbation theory with scale-dependent but local Lagrangian bias (Matsubara 2008b) is used for the real-space correlation function of halos, while the halo infall velocity and dispersion computed in standard perturbation theory with scale-independent bias. In order to go from halos to galaxies, Reid et al. (2012) showed that it suffices to introduce a single additional parameter, σ_{FOG}, akin to the σ_E in Eq. (1). This is taken to be an isotropic, scale-independent dispersion which is added in quadrature to σ_{12} and modifies the scale-dependence of the quadrupole moment on small scales.

2.4 The Lagrangian streaming model

The Lagrangian streaming model (LSM) is a hybrid model based upon the work in Reid & White (2011); Reid et al. (2012); Carlson, Reid & White (2013); Wang, Reid & White (2013); White (2014). It uses the Zel'dovich approximation (Zel'dovich 1970) with a model for local Lagrangian bias introduced by Matsubara (2008a,b, 2011) to predict the real-space correlation function of biased tracers. This model predicts the real-space statistics very well, compared to N-body simulations, but fares less well for the redshift-space statistics of biased tracers, particularly the quadrupoles. For this reason the real-space correlation function is "convolved" with a Gaussian as in Eq. (5), except that the dispersion is computed from Lagrangian rather than Eulerian perturbation theory and we shall denote it as σ_L. As discussed extensively in Reid & White (2011), the measured quadrupole is very sensitive to the pairwise velocity, v_{12}. For this reason we use the 1-loop expansion for v_{12} rather than just the lowest order (i.e. Zeldovich) term. [Comparison of this model with the full 1-loop calculation in Wang, Reid & White (2013) indicates that the differences are at the percent level on scales larger than $20\,h^{-1}$Mpc, except around the acoustic peak. Since the acoustic peak carries little weight in our fits we can treat the LSM and the model described in Wang, Reid & White (2013) as essentially identical, though the LSM is computationally easier.] As in the GSM, an additional parameter needs to be included to model fingers-of-god. We considered two approaches: an additional, isotropic, component to the Gaussian as in the GSM and an exponential form for the extra dispersion. In general we find that the exponential form produces almost identical results to the Gaussian form. Since the latter is easier to implement we shall use it throughout.

In principle the LSM depends on several parameters, but we choose to fix the bias parameters using the peak-background split expressions as described in White (2014). We have found that allowing the second bias parameter to float in the fits produces almost the same correlation functions as fixing it to the peak-background expression, so we work with the reduced parameter space. For a fixed linear power spectrum then, the final model depends on a single bias parameter, f and σ_L; i.e. the same number of parameters as the Eulerian model above.

2.5 Comparison

Figure 1 compares the monopole and quadrupole moments of the redshift-space correlation function of halos for the different theoretical models described above. We used the linear theory power spectrum appropriate to the T1 simulations (see Section 3) and a large-scale bias of $b = 2$ for all models, and have varied the finger-of-god parameters, σ_i, from $0.5\,h^{-1}$Mpc to $5\,h^{-1}$Mpc to illustrate their effects. Note that the σ_i have a much larger effect on the quadrupole than the monopole, altering small scales more than large. For such highly biased galaxies the effect of the finger-of-god modeling becomes comparable to the observational uncertainty for BOSS-like surveys below about $30\,h^{-1}$Mpc. The broadening of the acoustic peak in the Lagrangian models compared to the Eulerian models is clearly evident.

3 SIMULATIONS

In order to validate these different models we use mock catalogs derived from N-body simulations. Such validations have been performed for many of the models, often in the paper in which they were introduced, however our goal is to enable a side-by-side comparison using a common set of simulations, and to test the models for mock galaxies with properties similar to those of BOSS galaxies at $z \simeq 0.5$. We have created these mock catalogs from a number of different simulations, with differing cosmologies, codes and mock catalog generation methods (see Table 1 for a summary). While each is comparable to the BOSS data, the differing assumptions provide a good check of the models' ability to handle the complexities of how real galaxies trace the cosmic web.

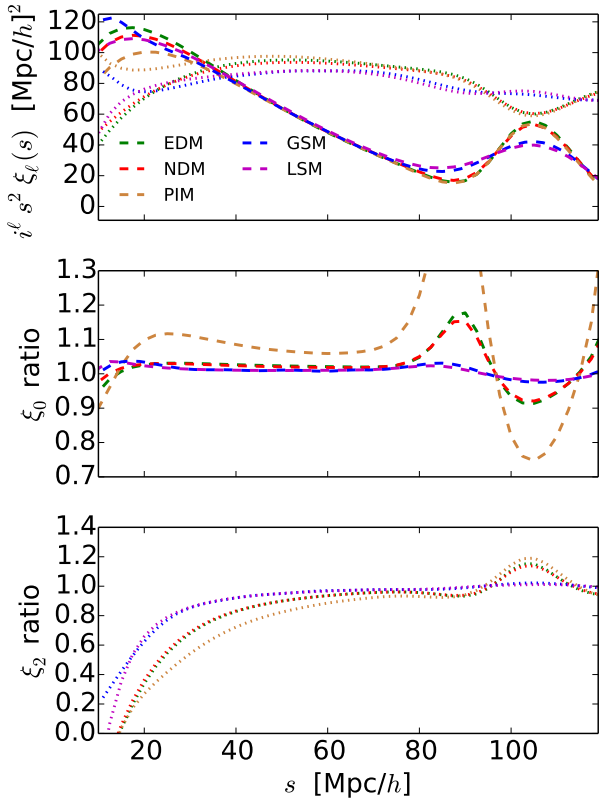

Figure 1. A comparison of the theoretical models described in Section 2. In the top panel the predictions for the monopole moment of the correlation function (multiplied by s^2 to reduce the dynamic range) are shown as dashed lines while those for the quadrupole moment are shown as dotted lines. We have taken the finger-of-god parameter, σ, to be small ($0.5\,h^{-1}$Mpc) to highlight the differences in the perturbative part of the models. In the lower panels we plot the ratio of the monopole and quadrupole moments with $\sigma = 5\,h^{-1}$Mpc to those with $\sigma = 0.5\,h^{-1}$Mpc to show the effects of varying σ. Generally, higher σ goes with a sharper "break" at small s in the quadrupole and lower clustering at small s in the monopole but σ has a much larger effect on the quadrupole than the monopole, and alters small scales more than large. For such highly biased galaxies the effect of the finger-of-god modeling becomes comparable to the observational uncertainty for BOSS-like surveys below about $30\,h^{-1}$Mpc. The broadening of the acoustic peak in the Lagrangian models compared to the Eulerian models is clearly evident. For the perturbation theory inspired model (PIM) we have set $A = 1$.

3.1 TreePM

The first set of simulations which we use (labeled T0 below) are those used in White et al. (2011); Reid & White (2011); Wang, Reid & White (2013); White (2014). The catalogs are based on twenty realizations of the ΛCDM model with $\Omega_m = 0.274$ and $h = 0.7$, each employing 1500^3 particles in a periodic box of side length $1500\,h^{-1}$Mpc for a total volume of $68\,h^{-1}$Gpc^3. The simulations were run with the TreePM code of White (2002) and the mock catalogs are described further in White et al. (2011). Briefly, halos were found using the friends-of-friends algorithm and populated with galaxies resembling those of BOSS using a halo occupation distribution (HOD). Each central galaxy was placed at the minimum of the halo potential and given a velocity equal to that of the halo center-of-mass, while halo particles were picked at random to model satellite galaxies.

Name	Ω_m	h	$f^{(0.55)}$	$\sigma_8^{(0.55)}$	$\bar{n}$	Vol
T0	0.274	0.70	0.74	0.61	3.6	68
T1	0.292	0.69	0.76	0.62	4	26
MD	0.307	0.68	0.77	0.61	4	16
QPM	0.290	0.70	0.76	0.61	4.1	268

Table 1. A summary of information about the simulations used in this paper (see text for further discussion). Each is of the ΛCDM family with the indicated values of the matter density (Ω_m) and Hubble parameter (h). We use a single redshift output to build the mock catalogs, which is near $z = 0.55$. The growth rate at this redshift, $f = d\ln D/d\ln a \approx \Omega_m^{0.55}$ where $D(a)$ is the linear theory growth factor. The normalization of the linear theory power spectrum at $z = 0.55$ is given in terms of $\sigma_8(z = 0.55)$, denoted $\sigma_8^{(0.55)}$. Finally we give the average number density, in $10^{-4}\,h^{-3}$Mpc^3, and the total volume, in h^{-3}Gpc^3, used in the computation of ξ_ℓ. For model T1 we have three variants (00, 01 and 10) which are described further in the text.

A second set of simulations (labeled T1), run with the same code, is also used (these simulations have also been used in Reid et al. 2014). This set has less volume but higher mass and force resolution and a different cosmology. This set consists of ten realizations of a ΛCDM model with $\Omega_m = 0.292$ and $h = 0.69$, each employing 2048^3 particles in a periodic box of side length $1380\,h^{-1}$Mpc. At each output of the simulation, two sets of halo catalogs were constructed. The first is based on the friends-of-friends algorithm as above. The second uses a spherical overdensity criterion. As before a HOD was used to generate mock galaxies. For the friends-of-friends halos, central and satellite galaxies were placed in the halo as above, except for one of the simulations (labeled 01) the satellite velocities were boosted by 25 per cent while in the base simulation (labeled 00) they were not. For the spherical overdensity catalog (labeled 10) the central galaxies were placed at rest compared to the inner region of the halo, rather than the halo center-of-mass. Since massive halos contain significant kinematic substructure, these prescriptions can differ by a fair fraction of the halo velocity dispersion, and generate differing amount of small-scale redshift-space distortions. Taken together these simulations explore a range of cosmologies and galaxy velocity prescriptions, as will be seen in the clustering statistics. We generated some other variants of these models, but in all cases the results were consistent with those we explore in more detail below so we focus on the models listed from now on.

Especially for the higher resolution simulations, the box size is not optimal for resolving features (such as the baryon acoustic peak) at $> 100\,h^{-1}$Mpc. Since $100\,h^{-1}$Mpc is about 10 per cent of the side length of the periodic box the missing long-wavelength modes have an impact on the correlation function and the large-scale velocities which act to broaden the acoustic peak. Fortunately, most of the RSD signal comes from smaller scales so this is not a major concern for the purposes of this work.

Due to the combination of large volume and high force and mass resolution we shall take the T1 simulations as our fiducial choice in the figures below, and we will comment specifically when the results from the other simulations show a qualitatively different behavior. We shall also use the SO catalog (denoted 10 above) as our fiducial model, as this catalog provides a very good match to the projected correlation function and monopole and quadrupole moments of the redshift-space correlation function of CMASS galaxies in BOSS (Reid et al. 2014).

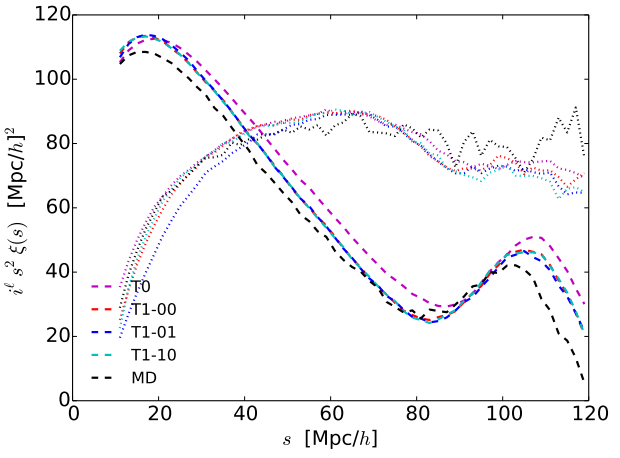

Figure 2. The monopole and quadrupole moments of the correlation function, times s^2 to reduce the dynamic range in the plot, for the simulations described in the text (see also Table 1). In each case the mean value of the statistic is plotted, in bins of width $2\,h^{-1}$Mpc, and error bars have been suppressed for clarity. Models T0 and T1 are described in section 3.1 while MD is described in section 3.2. Model T1 has three variants, which differ in terms of the halo finder and whether a velocity bias is assumed for the satellites.

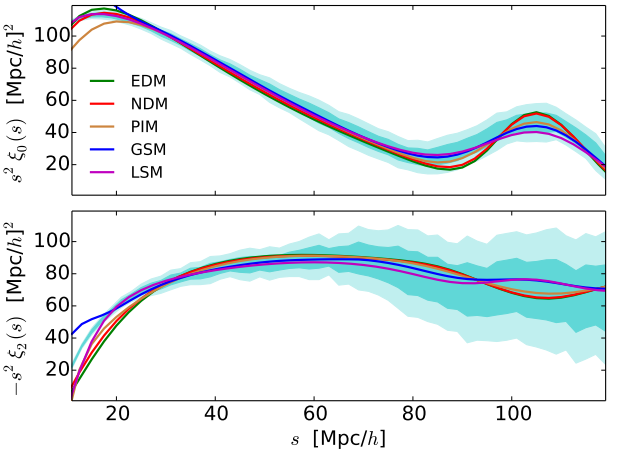

Figure 3. The best-fit models to the T1 simulation at $z \simeq 0.55$. Each model was fit to the data in the range $30 < s < 120\,h^{-1}$Mpc, holding the linear theory power spectrum and f fixed at the appropriate values for this simulation. The shaded bands around the simulation results indicate the adopted 1 and $2\,\sigma$ errors, derived from the diagonal elements of the covariance matrix. The error bars are highly correlated. The sharper acoustic peak in the monopole of the Eulerian models than the Lagrangian models is expected, as the Eulerian models do not account for non-linear broadening of the peak. Some of the modes which are responsible for this broadening are not captured by the T1 simulations, so the N-body peak is not as broad as it should be. The models are quite similar in their monopole predictions at intermediate scales however and the large scales carry little weight in the fit.

3.2 Big MultiDark

A further set of mock catalogs were generated from the "Big MultiDark" (hereafter BigMD or MD) simulation. This simulation employed 3840^3 particles in a periodic box of side length $2500\,h^{-1}$Mpc. The cosmology was close to the best-fitting Planck cosmology (Planck collaboration 2014), with $\Omega_m = 0.307$. Unlike the halo occupation based methods described above, these catalogs were produced by halo abundance matching as described in Nuzza et al. (2013), with galaxies associated to substructures. This has a more complex, and possibly realistic, velocity distribution than the HOD models above. Unfortunately the total volume of this simulation is only slightly larger than our fiducial mock survey (see below) so significant finite-volume 'noise' remains.

3.3 Quick particle mesh

Later we will use a set of *approximate* mock catalogs, which were run in order to generate covariance matrices for the BOSS measurements via Monte-Carlo techniques (see White, Tinker & McBride 2014, for further discussion). These mock catalogs use low mass and force resolution particle-mesh simulations employing 1280^3 particles in a $2560\,h^{-1}$Mpc box run with large time steps. At select times the particles, and their local density smoothed on $2\,h^{-1}$Mpc scales, were dumped and these particles were then sampled (with a density-dependent probability) to form a set of mock halos which are then populated using a halo occupation distribution (White, Tinker & McBride 2014). These approximate mock catalogs contain roughly the right amount of monopole and quadrupole power, but deviate from the high resolution simulations on scales smaller than $30 - 50\,h^{-1}$Mpc. We shall use these very large volume simulations, in a differential manner, to test the impact of observing strategy on the recovered cosmological parameters.

4 COMPARISON

4.1 Ideal data

We begin by asking to what extent each of our models can recover the simulation parameters when applied to "ideal" data. To this end we generate correlation functions from fixed-time outputs of the simulations assuming no observational non-idealities. For the TreePM and QPM runs we use the periodic outputs and generate a mean and variance for each point from the independent runs. For the BigMD run, we divide the $2500\,h^{-1}$Mpc box into its 8 octants and compute the correlation function in each octant, using the octants to determine the mean and variation on the parameters.

We show the monopole and quadrupole moments of the mock galaxies for a selection of the catalogs in Fig. 2. Note that the small scale behavior of the quadrupole moment depends upon the model chosen for the satellite and central velocities, while the amplitude of the monopole moment is largely set by mimicking the BOSS data. The range of slopes and behaviors reflects the differences in the underlying cosmology, linear power spectrum and bias prescription and makes for a good test of the theoretical models.

In order to provide fits to the data we need a covariance matrix. We use the linear theory expressions[1] (Bernstein 1994; Eisenstein & Zaldarriaga 2001; Cohn 2006; Huff et al. 2007)

$$\begin{aligned}\mathrm{Cov}\left[\xi_{\ell_1}(s_1), \xi_{\ell_2}(s_2)\right] &= \frac{2}{V} i^{\ell_1+\ell_2}(2\ell_1+1)(2\ell_2+1)\int \frac{d^3k}{(2\pi)^3} \\ &\times P^2(k,\mu) L_{\ell_1}(\mu) L_{\ell_2}(\mu) j_{\ell_1}(ks_1) j_{\ell_2}(ks_2) \quad (6)\end{aligned}$$

in order to generate a correlation matrix (sometimes referred to as

[1] The formula given assumes infinitesimal bins. We additionaly account for the finite bin width by integrating $s^2\, j_\ell$ over the bin.

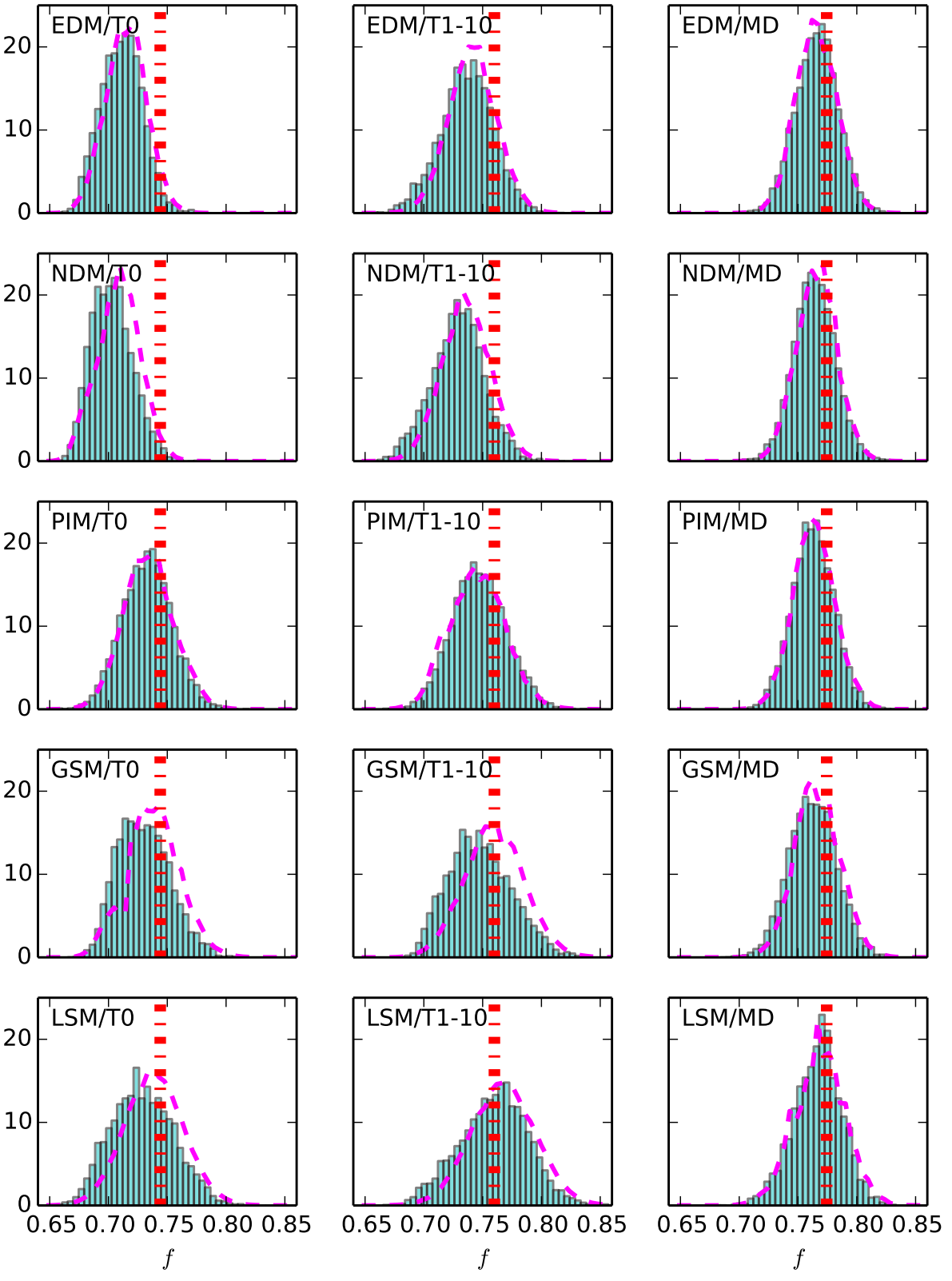

Figure 5. The profile likelihood (dashed lines) and the marginalized posterior distribution of f (filled histogram; from a Monte-Carlo Markov Chain), for the models described in Section 2 and the simulations described in Section 3. Scales larger than $30\,h^{-1}$Mpc have been fit, as described in the text. The vertical line marks the value of f appropriate to each cosmology.

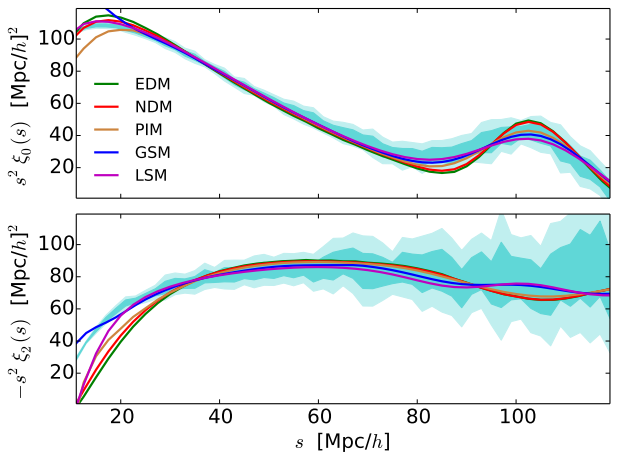

Figure 4. As in Fig. 3 but for the BigMD simulation at $z \simeq 0.56$. The error bars are highly correlated and the noise from the smaller total volume is apparent.

a reduced covariance matrix). Comparison of the linear theory correlation matrix with that produced from the QPM mock catalogs shows they are quite similar in structure (see also Reid et al. 2012). The correlation matrix is independent of the volume of the survey or any scaling of the bins (e.g. whether it is $s^2\xi_0$ or ξ_0 that is being constrained). The covariance matrix we use is then obtained from the linear theory correlation matrix by multiplying each row and column of the correlation matrix by the standard deviation per bin, measured from the independent simulations or octants, scaled (with error $\propto V^{-1/2}$) as if for a 5 $(h^{-1}\mathrm{Gpc})^3$ volume, roughly the volume expected for high-z galaxies in the final BOSS dataset. This ensures that we can assess sub-σ systematics with respect to the BOSS data but we are not simply fitting noise from the finite number of mock catalogs (since the volume of the mocks exceeds 5 $(h^{-1}\mathrm{Gpc})^3$ in all cases). By matching the error bars to those expected from BOSS we can also assess how degeneracies and nuisance parameters affect the fits in a way relevant to BOSS. In preparing these matrices and ξ_ℓ measurements we cover $10 < s < 120\,h^{-1}$Mpc using $2\,h^{-1}$Mpc bins[2]. We work with the first two even multipole moments, ξ_0 and ξ_2. In order to drop points at low or high s we simply add a large number to the nominal error bar before computing the covariance matrix and its inverse. This provides a simple way of restricting the fitting range which requires minimal changes to the code (though it does not fully remove the influence of the small scale points, which requires zeroing the correlations, but when the model is close to the data the difference is small and the approximation does not qualitatively affect our conclusions).

We begin by fitting the models with the "correct" linear theory power spectrum and cosmology (although we allow f to float in order to see if we recover the correct value). Since the distance scale and the shape of the power spectrum are not allowed to vary this test is quite constraining. There is no "slop" from other parts of the theory to hide a bad fit. Our nominal fitting range for most models is $30 < s < 120\,h^{-1}$Mpc. For the BigMD simulation the internal error estimate from the 8 octants becomes unreliable at the largest scale so we truncate the fit at $100\,h^{-1}$Mpc. For the EDM and NDM models we wish to avoid fitting the acoustic peak region entirely, since the shape of the peak is much sharper than seen in the N-body simulations (where the peak is broadened by non-linear evolution). As the peak height can be lowered, in these models, by increasing f the fits become highly unstable to large f if the peak is included in the fit. Thus we include only $s < 80\,h^{-1}$Mpc for these two models. Note that the acoustic peak region is not very important for this test as we are holding the cosmology and linear power spectrum fixed and the relative error on the large scale points is much larger than those at smaller scales. For a more general fit information from the acoustic peak would need to be included in some manner (e.g. as a prior on distance).

Figures 3 and 4 show how well the models fit the monopole and quadrupole moments measured from the T1 and BigMD simulation at $z \simeq 0.55 - 0.56$. (The situation is qualitatively very similar for the other mock catalogs.) The behavior of the models near the acoustic peak has been discussed previously. Some of the modes which are responsible for the broadening of the acoustic peak at $s \simeq 110\,h^{-1}$Mpc are not captured by the T1 simulations, so the N-body peak is not as broad as it should be. The simulation is well converged at intermediate scales, however, and the large scales carry little weight in the fit. The noise from finite volume is evident in the BigMD simulation.

Note that the Eulerian models predict a higher (i.e. more negative) quadrupole at large scales ($40\,h^{-1}\mathrm{Mpc} < s < 80\,h^{-1}\mathrm{Mpc}$) with a sharper "break" at small scales than the Lagrangian models, and in particular they underpredict the N-body data on scales below $30\,h^{-1}$Mpc. On the tens of Mpc scales which dominate the fits the GSM and LSM agree very well and agree quite well with the N-body data. All of the models predict very similar behavior for the monopole over the range $30\,h^{-1} < s < 70\,h^{-1}$Mpc and in particular the N-body monopole is well matched by all of the models in this range.

We can look for any biases or instabilities in the fit using a Monte-Carlo Markov Chain. We run several such chains with a parallel implementation of the affine-invariant ensemble sampler described in Goodman & Weare (2010). To begin we allow f, the bias and the finger-of-god parameter to vary at fixed linear power spectrum, with infinitely wide, flat priors[3].

The marginalized posterior distribution for f is shown in Fig. 5 for the models and simulations (Fig. 6 highlights the T1 simulations not shown here). The linear theory power spectrum has been held fixed and the other two parameters, bias and finger-of-god dispersion, have been marginalized over. We also show the profile likelihood (Wilks 1938), i.e. the value of the best fit at fixed f, allowing the large-scale bias and finger-of-god parameter to vary. This statistic provides information on the goodness of fit which is not affected by parameter volume effects. As we shall see, the agreement between the posterior and profile likelihood is reasonably good in all cases indicating that our posterior likelihoods are not unduly misleading due to volume effects, but we shall return to this point below.

The models all fare reasonably well for all simulations, but biases are visible at the $1\,\sigma$ level for several models. While they fare well for the BigMD simulation, the EDM and NDM models are biased slightly low for T0 and T1-10. This is a consequence of the mismatch in the quadrupole (compared to the other theories) seen in Fig. 1. The perturbation-inspired model performs well for all of

[2] We have tested that increasing the bin width to $4\,h^{-1}$Mpc does not alter the results.

[3] Except for the GSM model where we imposed a prior $\sigma < 10\,h^{-1}$Mpc for numerical reasons.

the simulations and the Lagrangian models do not show evidence for bias for any of these simulations either: the distribution of f values inferred from the fit is very well centered on the correct value for most simulations.

Since we are fitting our models to correlation functions measured from finite simulation volumes, we expect some scatter between the peak of the likelihood and the 'true' values, even in the case of a perfect model. The size of the typical offset should roughly be $\sqrt{V_5}\sigma_f$ where V_5 is the total volume of the simulations in units of our fiducial volume, $5\,h^{-3}\mathrm{Gpc}^3$.

For the T1 simulation we generated three catalogs which differ in the way dark matter halos are identified and populated with mock galaxies (see section 3.1). We compare the f distributions in Fig. 6. Again the simpler Eulerian models tend to lie slightly low while the other models tend to perform better. This is quite a significant test of our simple, 1-parameter finger-of-god prescription. As shown in Fig. 2, the shape of the quadrupole at small scales is different between the catalogs and yet the value of f is well recovered in all cases. This indicates that our simple 1-parameter finger-of-god prescription is adequate to describe the effects of such galaxy motions on scales above $30\,h^{-1}$Mpc.

In all of the above comparisons the posterior distribution of f for the EDM and NDM models lie low compared to the true value of f in the T1 simulation. We now examine how the fits behave as we vary the minimum scale in the fit, $s_{\rm min}$. Fig. 8 shows the posterior distribution of f for the minimum s of both the monopole and quadrupole varying $s_{\rm min}$ from 20 to $40\,h^{-1}$Mpc (the larger value is the range over which they have typically been used Chuang et al. 2013; Sanchez et al. 2013, 2014).

We see the expected behavior, an increasing bias but tighter distribution as we lower $s_{\rm min}$. For all models but LSM the bias at $s_{\rm min} = 20\,h^{-1}$Mpc is significant. While LSM appears to fare well in this test, the bias for this model can rise to $1\,\sigma$ for other simulations in the T1 series (specifically model 01, with enhanced satellite galaxy velocities). Increasing $s_{\rm min}$ to $24\,h^{-1}$Mpc when fitting the LSM returns unbiased fits for all catalogs, with the exception of T1-00. For this model the likelihood is broad and centered roughly $1\,\sigma$ higher than the 'true' value in the simulation. The difference in χ^2 between the best fit value of f and the 'true' value is small however ($\Delta\chi^2 < 1$) suggesting that the model does not rule out the correct value of f. For this reason, we see no evidence that the LSM cannot be used down to $\simeq 25\,h^{-1}$Mpc.

As we increase $s_{\rm min}$ we see generally less bias and a wider posterior distribution, though the bias remains significant for EDM and NDM even at $40\,h^{-1}$Mpc. The behavior of the LSM is at first sight surprising, because the bias appears to increase with increasing $s_{\rm min}$. This can be traced to the positive correlation between f and the finger-of-god parameter, σ, shown in Fig. 7 (see also the discussion in Reid et al. 2012). As we increase $s_{\rm min}$ the finger-of-god parameter becomes less constrained, and newly allowed low values of σ correspond to lower values of f. The peak of the marginal distribution thus shifts to lower f. If we had a well motivated prior for σ this degeneracy would be less important. For instance, Reid et al. (2014) propose a Gaussian prior on σ^2 around $14\pm5\,(h^{-1}\,\mathrm{Mpc})^2$. As shown in Fig. 7, this prior disfavors low values of σ, corresponding to models in which the galaxies have small intra-halo velocities inconsistent with the observed anisotropic clustering on small scales. Application of this prior shifts the central marginalized value of f upwards by $\sim 0.3\sigma$ (thus removing the small bias evident in Figs. 6 and 5) and reduces its uncertainty by 25 per cent. Since the other mock catalogs have purposely not been tuned to match the observed

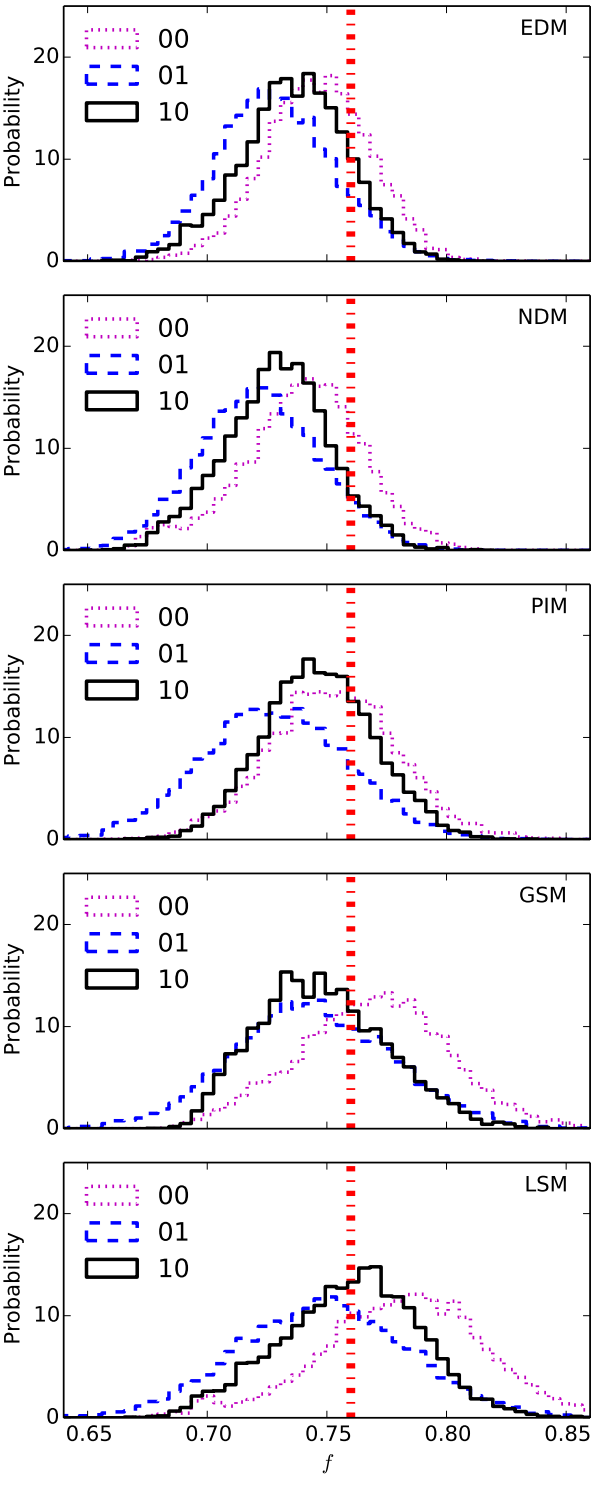

Figure 6. The marginalized posterior distribution of f for models built upon the T1 simulation, which have different prescriptions for how central and satellite velocities are assigned and different halo finding schemes (the numbering is described in Section 3: 00 uses the friends-of-friends halo center-of-mass velocity for the central galaxy, 01 enhances satellite velocities by 25 per cent and 10 is our fiducial model with SO halos). As in the earlier figures, the vertical line marks the value of f appropriate to this cosmology at $z \simeq 0.55$ and the data were fit over the range $30 < s < 120\,h^{-1}$Mpc. As the T1 simulations cover about five times our fiducial $5\,(h^{-1}\mathrm{Gpc})^3$ we expect shifts of around $0.5\,\sigma$.

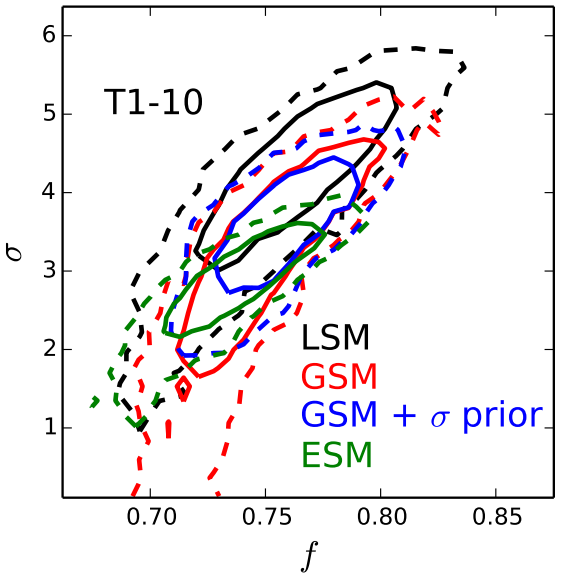

Figure 7. The marginalized joint posterior distribution of f and σ for the T1-10 mock for the LSM (black), GSM (red), and EDM (green) models. In each case there is a positive correlation between f and σ. If we apply the prior on σ advocated in Reid et al. (2012) for the GSM model, low values of σ are disfavored (blue). The central value of f shifts by $\sim 0.3\,\sigma$ and the uncertainty on f is reduced by 25 per cent after the application of the σ prior.

small scale anisotropic clustering, the proposed prior is not applicable to those mock samples and we have not attempted to use it.

The tests presented above are quite stringent, as they allow only a minimum number of parameters to vary. It is also of interest to ask how well the models perform when we allow the linear theory power spectrum and cosmological parameters to vary. In Fig. 9 we show the marginalized posterior for f from the LSM model, allowing the linear theory power spectrum to vary within a CMB prior as in Samushia et al. (2014). Specifically we allow $\omega_c \equiv \Omega_c h^2$, $\omega_b \equiv \Omega_b h^2$, n_s, $f\,\sigma$ and the large-scale bias to vary with a prior on ω_c, ω_b and n_s. We hold h and σ_8 fixed at their fiducial values. As discussed extensively in Reid et al. (2012); Samushia et al. (2013, 2014) within the ΛCDM family current CMB data tightly constrain the linear theory power spectrum so that allowing it to float or holding it fixed return almost the same marginalized constraints on f. This is clearly illustrated by Fig. 9.

4.2 Observational effects

The above tests have been performed on "ideal" measurements, involving constant time outputs, with constant number density done in periodic boxes. We now turn to a discussion of how departures from this ideal situation affect measurements of the growth rate.

In this section we make use of the QPM mock catalogs, in a differential fashion. We compare the ξ_ℓ measured on the constant time, uniform density, periodic QPM boxes to that computed on catalogs which have been projected onto the sky and observed under various constraints. We shall call these latter catalogs sky mocks. Throughout we shall work with the average of 100 sky mocks, sufficient to look for effects at much less than the expected

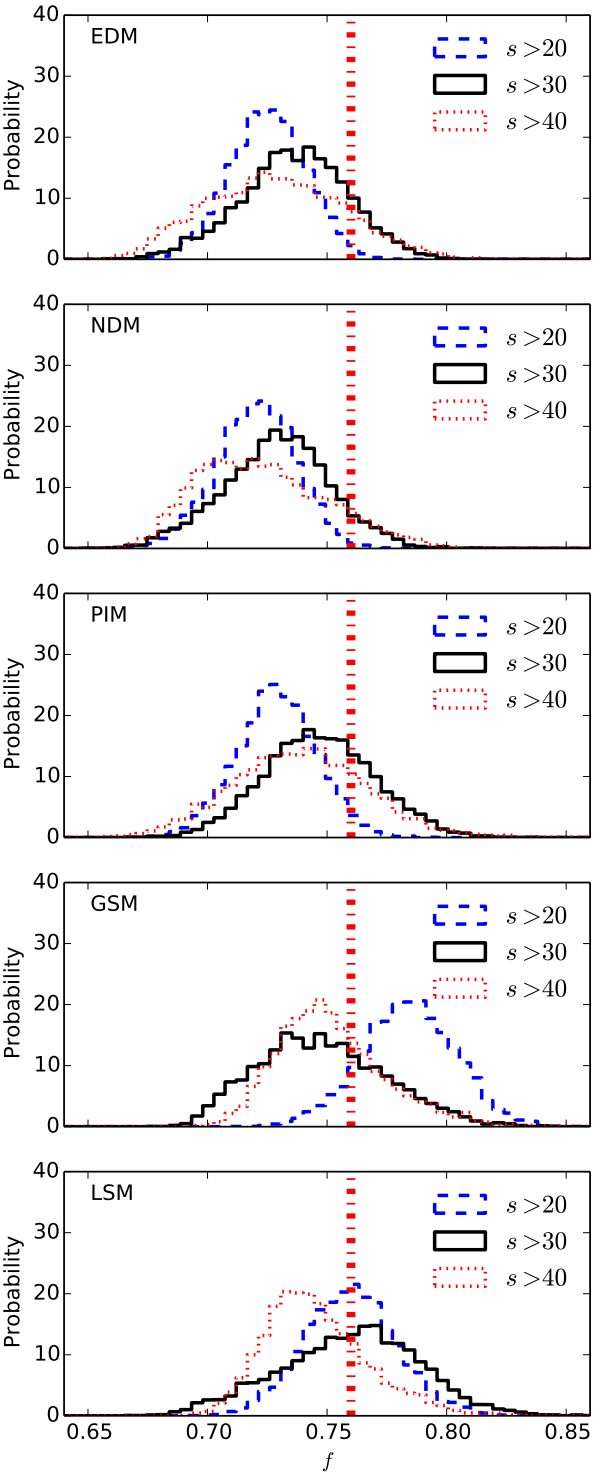

Figure 8. The marginalized posterior distribution of f as a function of the minimum scale in the fit (in h^{-1}Mpc) for each theoretical model. Again the T1-10 simulation is used and the vertical line marks the value of f appropriate to this cosmology at $z \simeq 0.55$. A similar behavior is seen for the other simulations (see text).

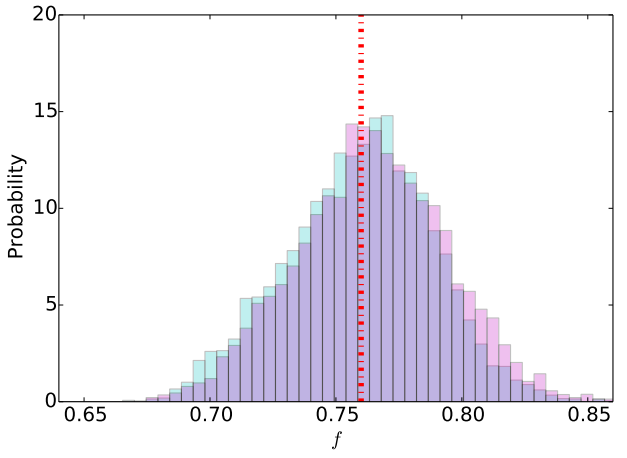

Figure 9. The marginalized posterior distribution of f for the fiducial cosmology allowing the linear theory power spectrum (and cosmological parameters) to vary within a CMB prior (magenta histogram) compared with the case of $P_{\rm lin}(k)$ fixed (cyan histogram). Within the ΛCDM family current CMB data tightly constrain the linear theory power spectrum, so that the constraints with fixed $P_{\rm lin}(k)$ or with a CMB prior are almost identical. Again the vertical line marks the value of f appropriate to this cosmology at $z \simeq 0.55$.

statistical error of BOSS. We now show that the effects on ξ_ℓ (and the covariance matrix) at the relevant scales are unimportant.

First we compare the average correlation function of the sky mocks to that of the periodic mocks, assuming no fiber collisions, redshift failures or systematics. The major differences are from the shape of $\bar{n}(z)$ and (to a lesser extent) wide-angle redshift-space distortions. We convert angles and redshifts to distances using the proper cosmology for the simulations, use the correlation function estimator of Landy & Szalay (1993) and assign redshifts to random points by 'shuffling' the data redshifts, which is the technique used in most of the BOSS papers to date. We use twenty times as many randoms as data points.

The average ξ_ℓ from the sky and periodic mocks differ by a small but measurable amount, even on large scales. This major driver of this difference is the redshift distribution chosen for the random points. This has been studied before, most recently by Samushia, Percival, & Raccanelli (2012). Those authors showed that our approach gives the smallest error for a wide-angle survey like BOSS, but this error is not negligible. Luckily the error is very small (less than 1 per cent) on the smallest scales and grows more slowly than the statistical error as we move to larger scales. Since our measurements are heavily weighted to small scales this effect is actually less important for redshift-space distortions than for e.g. anisotropic fitting of the baryon acoustic oscillation peak. Over the range $20 - 60\,h^{-1}$Mpc the effect is always less than 2.5 per cent, in both the monopole and quadrupole moments of the redshift-space correlation function. This is much less that our assumed statistical errors and comparable to the systematics from the modeling.

Next we introduce 'fiber collisions'. To mimic this observational effect we divide the mock galaxies into those which have a neighbour within 62″ and those which do not. We measure from the BOSS sample, as a function of position on the sky, the fraction of close pairs where one galaxy precluded the other getting a redshift. For each mock pair at the same sky position we randomly remove one galaxy from the pair, increasing the weight of its neighbor by one. If a galaxy has more than one near neigbhor we choose one at random. This is only an approximation to the fiber assignment scheme employed by BOSS on the real data (Blanton et al. 2003), but it captures the main features of the effect.

In common with earlier work (see e.g. Reid et al. 2014, for a recent study) we find that fiber collision correction using nearest neighbors has little impact on the correlation function on large scales. The monopole of the redshift-space correlation function is affected by less than one per cent on scales above $10\,h^{-1}$Mpc while the quadrupole is affected by less than one per cent above $30\,h^{-1}$Mpc and only by two per cent at $20\,h^{-1}$Mpc. Both of these errors are comfortably below the statistical and modeling error and can be ignored.

Next we discuss the impact of evolution across the sample, and the approximation inherent in interpreting our measurement as ξ_ℓ 'at' a given redshift.

4.3 Lightcone evolution

If the number density is slowly varying with redshift over the scales which dominate our fits[4], the correlation function we measure is (Matarrese et al. 1997; White, Martini & Cohn 2008)

$$\xi_{\ell,\rm obs}(s) \simeq \frac{\int dz\,(dN/dz)^2(H/\chi^2)\xi_\ell(s,z)}{\int dz\,(dN/dz)^2(H/\chi^2)} \qquad (7)$$

where dN/dz is the redshift distribution of the sample, H is the Hubble parameter at redshift z and χ is the comoving angular diameter distance to redshift z.

To get a sense for the amount by which evolution could change the shape of the correlation functions we assumed a Gaussian dN/dz, centered at $z = 0.55$ and with varying widths. Using the LSM as "truth", and the cosmology of the BigMD simulation, we computed the integral and compared it to $\xi(r, z_{\rm eff})$ where $z_{\rm eff}$ is evaluated by an integral similar to Eq. (7) but with z in the numerator rather than $\xi(s, z)$. Figure 10 shows the range of values of the moments of the correlation function take on across the redshift range for two different assumptions about the bias evolution: passive evolution (Fry 1996) and constant bias. We expect the former to be a better approximation for BOSS galaxies, and we see predicts more constant clustering with redshift. Figure 11 compares the average correlation function multipoles to those evaluated at $z_{\rm eff}$. The ratio is very close to scale-invariant, and within a few percent of unity even for quite broad redshift windows (for comparison the dN/dz for the BOSS CMASS sample has approximately ten percent width). This suggests that we can safely interpret the measurements of the correlation function as at an 'effective' redshift with little impact on the cosmology.

5 DISCUSSION

A key probe of cosmological expansion and our theory of gravity is the growth of large-scale structure, as revealed in the clustering of galaxies observed in large redshift surveys. A growing understanding of the process of structure formation allows us to compare well-motivated models to data from ever larger surveys to provide tight constraints on deviations from the standard model of cosmology.

[4] We have explicitly checked that this is true for the BOSS DR12 data set by counting galaxy pairs and comparing to Eq. (7).

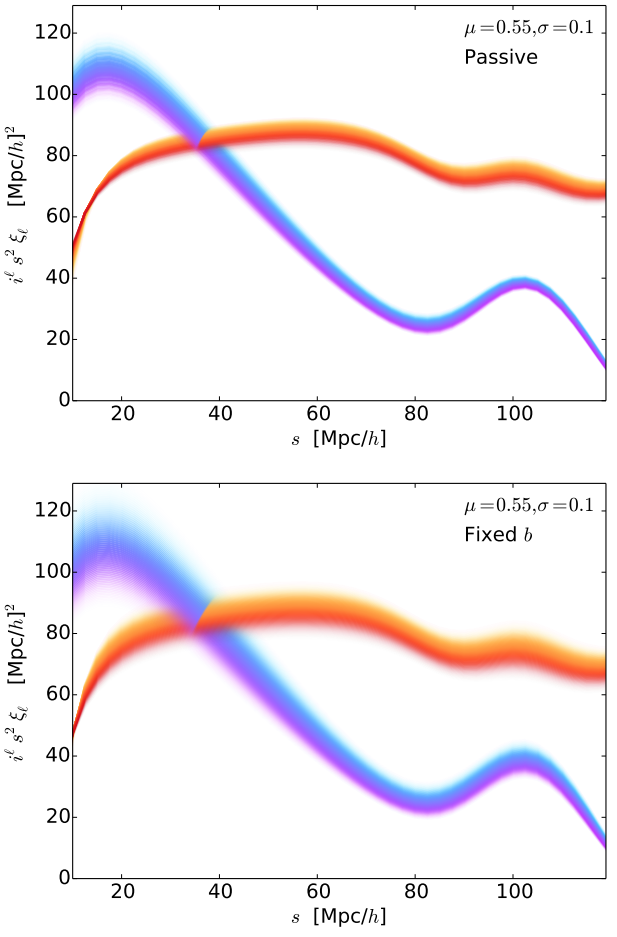

Figure 10. The evolution of the correlation function multipoles with redshift, as determined by the LSM for the cosmology of the BigMD simulation. In each panel the color scale indicates the redshift while the transparency scales with the weight in Eq. (7). The upper panel shows the result for a Gaussian dN/dz with the indicated mean and dispersion assuming passive evolution ($b-1 \propto D^{-1}$; Fry 1996) while the lower panel assumes fixed b. The former is a better approximation to the evolution of the clustering of BOSS galaxies (White et al. 2011).

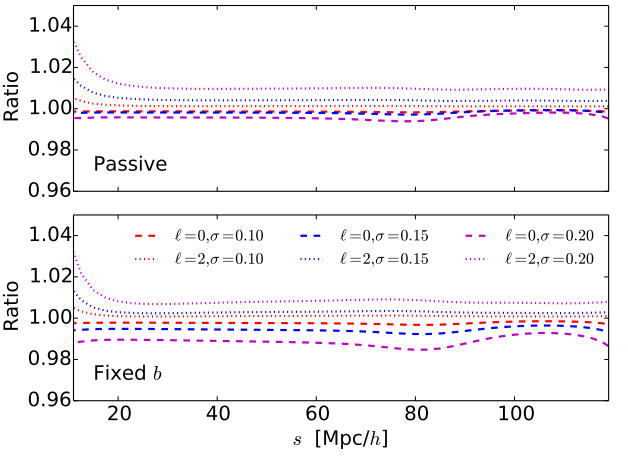

Figure 11. The ratio of the redshift-averaged correlation function multipoles to the model evaluated at $z_{\rm eff}$, i.e. using a constant-time approximation, for Gaussian dN/dz with the listed mean and standard deviation (for the $\sigma = 0.2$ case we have set $dN/dz = 0$ for $z < 0.05$). In all cases the ratio is nearly scale independent and close to unity.

In this paper we have compared the predictions from a number of phenomenological models for the anisotropic clustering of galaxies measured in configuration-space against a series of mock catalogs designed to mimic the high redshift sample from BOSS.

Even dealing with 'ideal' data, we have found that none of the proposed models fit the mock data on all scales, but they all do a good job of fitting the monopole and quadrupole moments of ξ in the range $40 < s < 80\,h^{-1}$Mpc. Dispersion models based on the simplest versions of Eulerian perturbation theory do not provide a good fit to the baryon acoustic peak feature of BOSS-like galaxies at $z \simeq 0.5$, but fare well on the shape of the monopole and quadrupole on intermediate scales. They tend to slightly underpredict the growth rate of structure when fit down to $20 - 30\,h^{-1}$Mpc scales.

More sophisticated models, and models based on Lagrangian perturbation theory, such as the GSM and LSM (Section 2), provide unbiased fits to the data on scales above $25 - 30\,h^{-1}$Mpc. In particular the LSM is straightforward and fast to compute and provides a reliable model for fitting BOSS-like galaxies at $z \simeq 0.5$.

Including non-idealities such as fiber collisions or lightcone evolution does not appreciably modify these conclusions. Using standard corrections for fiber collisions and interpreting the lightcone data as a measurement at an effective redshift introduces errors which are small compared to other sources of uncertainty.

M.W. would like to thank Chris Blake for helpful comments on an early draft of the manuscript. M.W. is supported by NASA. This work made extensive use of the NASA Astrophysics Data System and of the `astro-ph` preprint archive at `arXiv.org`. The analysis made use of the computing resources of the National Energy Research Scientific Computing Center. The MultiDark Database used in this paper and the web application providing online access to it were constructed as part of the activities of the German Astrophysical Virtual Observatory as result of a collaboration between the Leibniz-Institute for Astrophysics Potsdam (AIP) and the Spanish MultiDark Consolider Project CSD2009-00064. The BigMD simulation suite was performed in the supercomputer at LRZ.

REFERENCES

Planck Collaboration XVI; Ade P.A.R., et al., 2014, A&A, in press [arXiv:1303.5076]
da Angela J. et al., 2008, MNRAS, 383, 565
Baldauf T., Seljak U., Desjacques V., McDonald P., 2012, Phys. Rev. D86, 083540 [arXiv:1201.4827]
Ballinger W.E., Peacock J.A., Heavens A.F., 1996, MNRAS, 282, 877
Bel J., et al., 2014, A&A, 563, 37
Berlind A., Narayanan V.K., Weinberg D.H., 2001, ApJ, 549, 688.
Bernardeau, F., Colombi, S., Gaztañaga, E., Scoccimarro, R., 2002, Physics Reports, 367, 1
Bernstein G.M., 1994, ApJ, 424, 569
Beutler F., et al., 2014, submitted to MNRAS [arXiv:1312.4611]
Bianchi D., Guzzo L., Branchini E., Majerotto E., de la Torre S.,

Marulli F., Moscardini L., Angulo R.E., 2012, MNRAS, 427, 2420
Blake C., et al., 2011, MNRAS, 415, 2876
Blake C., et al., 2013, MNRAS, 436, 3089
Blanton M.R., Lin H., Lupton R., Maley F., Young N., Zehavi I., Loveday, J., 2003, AJ, 125, 2276
Bond J.R., Couchman H.M.P., 1988, in the Proceedings of the Second Canadian Conference on General Relativity and Relativistic Astrophysics, p. 385
Buchert T., 1989, A&A, 223, 9
Carlson, J., Reid, B.A., White, M, 2013, MNRAS, 429, 1674
Chan K.C., Scoccimarro R., Sheth R., 2012, PRD, 85, 083509
Chuang C.H., et al., 2013, MNRAS, 433, 3559.
Cohn J.D., 2006, New. Astron., 11, 226
Cole S., Fisher K., Weinberg D.H., 1995, MNRAS, 275, 512.
Coles P., Lucchin F., 1995, "Cosmology: the origin and evolution of cosmic structure", John Wiley & Sons (London, 1995)
Coles P., Melott A.L., Shandarin S.F., 1993, MNRAS, 260, 765
Coles P., Sahni V., 1996, The Observatory, v.116, p.25-31
Dawson K., et al., 2013, AJ, 145, 10
Doroshkevich A.G., Kotok E.V., Poliudov A.N., Shandarin S.F., Sigov Iu.S., Novikov I.D., 1980, MNRAS, 192, 321
Eisenstein D.J., Seo H.J., Sirko E., Spergel D.N., 2007, ApJ, 664, 675
Eisenstein D.J., et al., 2011, AJ, 142, 72
Eisenstein D.J., Zaldarriaga M., 2001, ApJ, 546, 2
Fisher K.B., 1995, ApJ, 448, 494
Fisher K.B., Nusser A., 1996, MNRAS, 279, 1
Fry J.N., 1996, ApJ, 461, L65
Gaztanaga E., Cabre A., Hui L., 2009, MNRAS, 399, 1663 [arXiv:0807.3551]
Gil-Marin H., Wagner C., Verde L., Porcini C., Jimenez R., 2012, J. Cosmol. Astropart. Phys., 11, 029
Goodman J., Weare J., 2010, CAMCOS, 5, 65.
Goroff M.H., Grinstein B., Rey S.-J., Wise, M.B., 1986, ApJ, 311, 6
Gorski K., 1988, ApJ, 332, L7
Gurbatov S.N., Saichev A.I., Shandarin S.F., 2012, Physics Uspekhi, 55, 223
Guzzo L., et al., 2008, Nature, 451, 541.
Hamilton A.J.S., "Linear redshift distortions: A review", in "The Evolving Universe", ed. D. Hamilton, pp. 185-275 (Kluwer Academic, 1998) [astro-ph/9708102]
Hatton S.J., Cole S., 1999, MNRAS, 310, 113
Hidding J., Shandarin S.F., van de Weygaert R., 2014, MNRAS, in press [arXiv:1311.7134]
Hivon E., Bouchet F.R., Colombi S., Juszkiewicz R., 1995, A&A, 298, 643
Huff E., Schulz A.E., White M., Schlegel D.J., Warren M.S., 2007, Astroparticle Physics, 26, 351
Jackson J., 1972, MNRAS, 156, 1
Jain B., Bertschinger E., 1994, ApJ, 431, 495
Jain B., Zhang P., 2008, Phys. Rev. D, 78, 063503
Jennings E., Baugh C.M., Pascoli S., 2011, MNRAS, 410, 2081
Jing Y.P., Börner G., 2004, ApJ, 617, 782
Juszkiewicz R., 1981, MNRAS, 197, 931
Kaiser N., 1987, MNRAS, 227, 1
Kazin E. et al., 2010, ApJ, 710 1444 [arXiv:0908.2598]
Kwan J., Lewis G.F., Linder E.V., 2012, ApJ, 748, 78
Landy S.D., Szalay A.S., 1993, ApJ, 412, 64
Li C., Jing Y.P., Kauffmann G., Börner G., Xi K., Wang L., 2007, MNRAS, 376, 984
Makino N., Sasaki M., Suto Y., 1992, Phys. Rev. D, 46, 585
Matarrese S., Coles P., Lucchin F., Moscardini L., 1997, MNRAS, 286, 115
Matsubara T., 2008a, Phys Rev D77, 063530
Matsubara T., 2008b, Phys Rev D78, 083519
Matsubara, T., 2011, Phys Rev D83, 083518
McCullagh N., Szalay A., 2012, ApJ, 752, 21
McDonald P., Roy A., 2009, JCAP, 0908, 020
McDonald P., Seljak U., 2009, JCAP, 10, 7
Melott A.L., Pellman T.F., Shandarin S.F., 1994, MNRAS, 269, 626
Moutarde F., Alimi J.-M., Bouchet F.R., Pellat R., Ramani A., 1991, ApJ, 382, 377
Munshi D., Sahni V., Starobinsky A.A., 1994, ApJ, 436, 517
Nesseris S., Perivolaropoulos L, 2008, Phys. Rev. D, 77, 023504
Noh Y., White M., Padmanabhan N., 2009, Phys. Rev. D80, 123501
Nuza S.E., et al., 2013, MNRAS, 432, 743.
Okumura T., et al., 2008, ApJ, 676, 889
Okumura T., Jing Y., 2011, ApJ, 726, 5
Okumura T., Seljak U., Desjacques V., 2012, JCAP, 11, 014
Okumura T., Seljak U., Vlah Z., Desjacques V., 2014, JCAP, 05, 003
Pauls J.L., Melott A.L., 1995, MNRAS, 274, 99
Padmanabhan N., White M., Phys. Rev. D80, 063508
Padmanabhan N., White M., Cohn J.D., 2009, Phys. Rev. D79, 063523
Park C., Vogeley M.S., Geller M.J., Huchra J.P., 1994, ApJ, 431, 569.
Peacock, J.A., 1992, MNRAS, 258, 581.
Peacock J.A., 1999, "Cosmological physics", Cambridge University Press (Cambridge, 1999)
Peacock, J.A., Dodds S., 1994, MNRAS, 267, 1020.
Peacock J.A. et al., 2001, Nature, 410, 169 [astro-ph/0103143]
Peebles P.J.E., 1980, "The large-scale structure of the Universe", Princeton University Press (Princeton, 1980).
Percival W.J. et al., 2004, MNRAS, 353, 1201
Percival W.J., White M., 2008, MNRAS, 393, 297
Porto R.A., Senatore L., Zaldarriaga M., 2014, JCAP, 05, 022 [arXiv:1311.2168]
Press W.H., Schechter P., 1974, ApJ, 187, 425
Reid B.A., White M., 2011, MNRAS, 417, 1913
Reid B.A., et al., 2012, MNRAS, 426, 2719 [arXiv:1203.6641]
Reid B.A., et al., 2014, in press.
Roth N., Porciani C., 2011, MNRAS, 415, 829
Sahni V., Coles P., 1995, Phys. Rep., 262, 1
Samushia L., Pericval W., Raccanelli A., 2012, MNRAS, 420, 2102
Samushia L., Reid B.A., White M., Percival W.J., et al., 2013, MNRAS, 429, 1514
Samushia L., Reid B.A., White M., Percival W.J., et al., 2014, MNRAS, 439, 3504 [arXiv:1312.4899]
Sanchez A., et al., 2013, MNRAS, 433, 1202.
Sanchez A., et al., 2014, MNRAS, 440, 2692.
Schulz A., White M., 2006, Astroparticle Physics 25, 172 [astro-ph/0510100]
Scoccimarro R., 2004, Phys. Rev. D, 70, 083007
Seljak U., 2001, MNRAS, 325, 1359.
Seto N., Yokoyama J., 1998, ApJ, 492, 421
Shandarin S.F., Zel'dovich Ya.-B., 1989, Reviews of Modern Physics, 61, 185
Sheth R., Chan K.C., Scoccimarro R., 2012, Phys. Rev. D, 87, 083002 [arXiv:1207.7117]
Sheth R., Tormen G., 1999, MNRAS, 308, 119
Smith R.E., Peacock J.A., Jenkins A., White S.D.M., Frenk C.S.,

Pearce F.R., Thomas P.A., Efstathiou G., Couchman H.M.P., 2003, MNRAS, 341, 1311
Song Y.-S., Koyama K., 2009, JCAP, 1, 48
Song Y.-S., Percival W.J., 2009, JCAP, 10, 4
Song Y. S., Sabiu C. G., Nichol R. C., Miller C. J., 2010, JCAP, 1, 25 [arXiv:1001.1154]
Song Y. S., Sabiu C. G., Kayo I., Nichol R.C., 2011, JCAP, 5, 20 [arXiv:1006.4630]
Szalay A.S., 1988, ApJ, 333, 21
Tassev S., Zaldarriaga M., 2012a, JCAP, 4, 013
Tassev S., Zaldarriaga M., 2012b, JCAP, , 10, 006
Tassev S., Zaldarriaga M., 2012c, JCAP, 12, 011 [arXiv:1203.5785]
Tassev S., 2014a, JCAP, 06, 008 [arXiv:1311.4884]
Tassev S., 2014b, JCAP, 06, 012 [arXiv:1311.6316]
Taylor A.N., Hamilton A.J.S., 1996, MNRAS, 282, 767
Tinker J.L., Weinberg D.H., Zheng Z., 2006, MNRAS, 368, 85
Tinker J.L., 2007, MNRAS, 374, 477
Tojeiro R., et al., 2014, MNRAS, 440, 2222.
de la Torre S., Guzzo L., 2012, MNRAS, 427, 327
de la Torre S., et al., 2013, A&A, 557, 54
Vishniac E., 1983, MNRAS, 203, 345
Wang X., Szalay A., 2012, PRD, 86, 043508
Wang L., Reid B.A., White M., 2013, MNRAS, 437, 588
White M., 2001, MNRAS, 321, 1.
White M., 2002, ApJS, 579, 16
White, M., Blanton, M., Bolton, A., et al. 2011, ApJ, 728, 126
White M., Martini P., Cohn J.D., 2008, MNRAS, 390, 1179
White M., Song Y.-S., Percival W., 2009, MNRAS, 397, 1348
White, M., Tinker J.L., McBride, C.K., 2014a, MNRAS, 437, 2594
White, M., 2014, MNRAS, 439, 3630 [arXiv:1401.5466]
Wilks A.S.S., 1938, Ann.Math.Statist., 1, 60
Yoo J., Seljak U., 2014, preprint [arXiv:1308.1093]
Yoshisato A., Morikawa M., Gouda N., Mouri H., 2006, ApJ, 637, 555
Zel'dovich, Y., 1970, A&A, 5, 84
Zhang P., Liguoi M., Bean R., Dodelson S., 2007, Phys. Rev. Lett. 99, 1302
Zhao G.B., Giannantonio T., Pogosian L., Silvestri A., Bacon D.J., Koyama K., Nichol R.C., Song Y.S., 2010, PhRvD, 81, 103510 [arXiv:1003.0001]
Zheng Y., Zhang P., Jing Y., Lin W., Pan J., 2013, Phys. Rev. D88, 103510